CO methanation promoted by UV irradiation over Ni/TiO$_2$

Xiahui Lin [a,b], Liuliu Lin [a], Kun Huang [a], Xun Chen [a], Wenxin Dai [a,*], Xianzhi Fu [a,*]

[a] State Key Laboratory of Photocatalysis on Energy and Environment, Research Institute of Photocatalysis, Fuzhou University, Fuzhou 350002, China
[b] College of Chemistry & Material Science, LongYan University, Longyan 364012, China

ARTICLE INFO

ABSTRACT

Thermo-catalytic CO methanation has been widely investigated as an attractive strategy for the removal of CO in H$_2$-rich stream. In this paper, UV irradiation was introduced into the system of thermo-catalytic CO methanation over a noble-metal-free Ni/TiO$_2$ catalyst. It is found that UV irradiation can remarkably promote the CO conversion and CH$_4$ selectivity, as well as an excellent catalytic stability under the thermo-catalytic reaction conditions. Results of XPS, FT-IR, and TPO measurements for the Ni/TiO$_2$ catalyst indicate that upon UV light irradiation, the photo-generated electrons are transferred from the TiO$_2$ support to the adjacent Ni sites, and causes the Ni sites with increased surface electron density which subsequently enhances the adsorption and activation of CO molecules at Ni sites, and ultimately promotes the catalytic performance of CO methanation. This result shows that photo-excitation of TiO$_2$ can act as an electron donor to promote the thermo-catalytic performance of CO methanation over Ni/TiO$_2$.

© 2014 Elsevier B.V. All rights reserved.

1. Introduction

Hydrogen-fueled proton exchange membrane fuel cells (PEM-FCs) have been regarded as a promising power generator for directly converting chemical energy into electricity with high efficiency and cleanness [1–4]. At present, H$_2$ fuel is mainly supplied by steam reforming and partial oxidation of fossil fuels. However, the inevitably produced CO content (1–8%) in the resulted H$_2$ stream is high enough to poison the anode of PEMFCs (the tolerant CO concentration must be less than 50 ppm) [5–10]. Therefore, it is imperative to eliminate CO in H$_2$-rich stream for fuel cells applications [11].

One widely studied method for CO removal is the preferential oxidation of CO by introducing air; which however, employs extra devices for O$_2$ dosing, involves high reaction temperatures, and causes a high conversion of H$_2$ into H$_2$O to remove the CO below 100 ppm [12–14]. Another effective method to remove CO is the membrane separation process based on the diffusion of hydrogen through a Pd–Ag membrane, but this method requires a high pressure manipulation together with the costly membrane [15,16]. Advantaging over the above two approaches, the selective thermo-catalytic methanation of CO (3H$_2$ + CO = CH$_4$ + H$_2$O, $\Delta H = -206$ kJ mol^{-1}) is an attractive strategy for the removal of CO in H$_2$-rich stream, because it works without additional reactants or expensive units, consumes negligible amount of H$_2$ as long as the concentration of CO is very low, and produces inert diluent CH$_4$ that can be used as fuel to heat the stream reformer [17–21].

Various supported noble metal catalysts have been developed for the effective hydrogenation of CO to CH$_4$ [22–29]. Nevertheless, the rareness and the high cost of noble metals severely limit the long-term and large-scale applications of the catalysts. Alternatively, the supported Ni catalysts [5,30–34], especially TiO$_2$ supported Ni catalyst [35–38], have also shown excellent thermal catalytic performance for CO methanation, but with a higher reaction temperature than Ru/TiO$_2$. As to the reaction mechanism of CO methanation over the oxide-supported Ni catalysts, the generally accepted viewpoint is that the adsorption and activation of CO at active metal sites are the major determinants of the methanation of CO, consistent with that of the oxide supported noble metal catalysts [4,18,25,39]. Because the adsorption and activation of CO are favored over the metal nanoparticles with higher electron density [40–42], an approach to increase the surface electron density of metal nanoparticles should promote the methanation of CO. Considering that TiO$_2$ can be excited to produce photogenerated electrons under UV irradiation, we have ever introduced UV light into the thermo-catalytic reaction system for CO methanation over the TiO$_2$ supported noble metal Ru catalyst (Ru/TiO$_2$) [43], and found that UV irradiation exactly enhances the catalytic activity and stability for the hydrogenation of CO to CH$_4$. Moreover, the exploration of the reaction mechanism demonstrated that the promotional effect of UV light was attributed to the increased surface electron density of Ru nanoparticles induced by the electron

* Corresponding authors. Tel.: +86 591 83779083; fax: +86 591 83738608.
E-mail addresses: daiwenxin@fzu.edu.cn (W. Dai), xzfu@fzu.edu.cn (X. Fu).

transfer from the photo-excited TiO_2 support to the Ru sites. This result also shows that UV irradiation can decrease the operation temperature of CO methanation reaction over Ru/TiO_2.

In the present work, we have further introduced UV light to the thermo-catalytic reaction system of CO methanation over the noble-metal-free Ni/TiO_2 catalyst. It is expected that the photo-thermal catalytic coupling effect can also occur on the TiO_2 supported Ni catalyst. The results demonstrated that UV irradiation also significantly promoted the catalytic activity and stability of Ni/TiO_2 for CO methanation. Furthermore, we also proposed a possible reaction mechanism for the UV light enhanced CO methanation over Ni/TiO_2 catalyst.

2. Experimental

2.1. Catalysts preparation

The Ni/TiO_2 catalyst was synthesized by a facile impregnation-reduction method. The prepared TiO_2 sol [44] was first dried at 80 °C, followed by calcination at 450 °C in the air for 2 h to obtain the TiO_2 powder. Then, the TiO_2 powder (1.0 g) was immersed into a nickel nitrate solution (1.0 mL, 0.17 M) for 12 h at room temperature. After dried at 80 °C, the resulting powder was reduced by an aqueous $NaBH_4$ solution (50 mL, 0.1 M), and thoroughly rinsed with deionized water. Lastly, the powder was dried by a vacuum oven at 80 °C for 3 h, obtaining the Ni/TiO_2 catalyst with a theoretical Ni loading of 1.0 wt%. The actual loading of Ni is ca. 0.84 wt%, as determined by ICP-MS measurement. For the convenience of discussion and comparison with other work [43], we use the theoretical data (1.0 wt%) to denote the Ni loading of the Ni/TiO_2 catalyst in the following paper.

2.2. Catalyst characterization

X-ray diffraction (XRD) patterns were collected on a Bruker D8 Advance instrument (Cu Kα1 irradiation, λ = 1.5406 A). The accelerating voltage and the applied current were 40 KV and 40 mA, respectively. Data were recorded at a scanning rate of 0.02° 2θ s^{-1} in the 2θ region of 10–80°. Transmission electron microscopy (TEM) measurements were performed on a JEOL JEM-2010 EX with field emission gun a 200 kV. A micromeritics ASAP 2020 BET analyzer was employed to carry out the textual analysis of the samples by N_2 adsorption at liquid N_2 temperature. The samples were first degassed at 250 °C under vacuum for 4 h before analysis. The UV–vis diffuse reflection spectra (DRS) were measured on a Cary 500 UV–vis diffuse reflectance spectroscopy with $BaSO_4$ as the internal reflectance standard. A Thermo Scientific ESCALab250 spectrometer was used to collect the X-ray photoelectron spectroscopy (XPS) spectra of the samples. All of the binding energies were calibrated by the C1s peak at 284.6 eV. The temperature programmed oxidation (TPO) analysis was conducted on Micromeritics Autochem 2910 instrument. A Thermo Scientific X Series II inductively coupled plasma mass spectrometry (ICP-MS) system was used to determine the actual Ni loading of the Ni/TiO_2 catalyst.

2.3. Catalytic performance

The catalytic evaluations of the hydrogenation of CO to CH_4 were operated in a fixed-bed flow reactor under an atmospheric pressure. In the typical reaction, the Ni/TiO_2 catalyst (600 mg) with a grain size of 0.2–0.3 mm was packed in a flat-plate quartz cell (30 × 20 × 0.5 mm), and heated by an electric resistance board. The temperature of the catalyst bed was monitored by a K-type thermocouple inserted into the reactor. During the photo-thermal reaction process, UV light (produced by a 300 W Xenon lamp with a UV-reflectance filter, 300 nm < λ < 420 nm) was irradiated form the top

surface of the quartz cell. For the thermal reactions (without light), the quartz cell was enclosed by Al foils to rule out light irradiations. As the metallic Ni are easy to be oxidized with exposure to the air, before the photocatalytic reactions, the Ni/TiO_2 catalyst was first reduced at 300 °C by H_2 for 2 h with a flow rate of 30 ml min^{-1}. Then, the H_2 stream was switched to He stream, until the temperature was cooled down to room temperature. Finally, the feed stream (composition: 1 vol% CO, 3–40 vol% H_2, and the balance gas He) was fed at a total flow rate of 100 ml min^{-1}. The reactions were performed at the optimized operation temperature of 250 °C, after investigated the effect of reaction temperature on CO methanation over Ni/TiO_2 catalyst under UV irradiation or not (Fig. S1). The effluent stream was analyzed by an online Agilent 4890D gas chromatograph system equipped with a thermal conductivity detector (TCD) and a flame ionization detector (FID). The activity was evaluated by the conversion of CO, which could be calculated on the basis of the content change of CO in the feed and effluent stream:

$$CO conversion = (V_{inCO} - V_{outCO})/V_{inCO}.$$

The selectivity of CH_4 was calculated by the following equation:

$$CH_4 selectivity = V_{outCH4}/(V_{inCO} - V_{outCO}).$$

Here, V_{outCH4} denotes the volume of CH_4 in the effluent stream; V_{inCO} and V_{outCO} denote the volume of CO in the feed and effluent stream, respectively.

2.4. Chemisorption of reactants on catalysts

The chemisorption of CO on Ni/TiO_2 samples were measured on an FT-IR spectra instrument (Nicolet Nexus, Model 670) equipped with a controlled environmental chamber containing two CaF_2 windows. A self-supporting sample pellet (20 mg) was mounted on a holder in the chamber. Before tests, the sample was subjected a low-temperature reductive thermal treatment as follows: (1) heating to 150 °C under vacuum (10^{-4} Pa) for 1 h; (2) exposing to 200 Torr of H_2 at 250 °C for 1 h; (3) degassing at 250 °C for 1 h under vacuum. After cooling to room temperature, the absorption spectrum of sample was recorded as a reference. Then, CO was introduced into the chamber under the same controlled pressure. After 30 min, the absorption spectra of CO were collected. For testing FT-IR under UV irradiation, a UV light (300 W Xenon lamp with a UV-reflectance filter) was introduced onto the surface of the sample during the process of gas absorption. All spectra were recorded by a DTGS KBr detector in the transmission mode.

2.5. Temperature programmed oxidation (TPO)

Temperature-programmed oxidation (TPO) measurements of the samples were conducted to analyze the amount of elemental carbon (Ni–C) remained on the used Ni/TiO_2 catalysts after CO methanation reaction for 4 h under UV irradiation or not. The reaction conditions were identical to that described in Section 2.3 (feed stream composition: 1.0 vol% CO, 3.0 vol% H_2, and the balance gas He). After reaction for 4 h, the catalyst was cooled down to room temperature in a flow of He. For TPO testing, 100 mg of the used catalyst was packed in a quartz U-tube, flushed with He for 1 h at 400 °C to remove unconverted reactants and products, and then cooled down to room temperature slowly, followed by continuing purge with He overnight. Subsequently, a stream of 50 vol% O_2 in the He (30 mL min^{-1}) was passed through the sample with a temperature-rising rate of 10 °C min^{-1} from 25 to 450 °C. Meanwhile, the mass spectrometry (MS) analysis was performed to monitor the consumption of O_2 and the formation of CO_2 (m/z values of 32 and 44, respectively).

Table 1
The textural data of TiO_2 and Ni/TiO_2 samples.

| Sample	S_{BET} ($m^2\,g^{-1}$)	Pore volume ($mL\,g^{-1}$)	Pore diameter (nm)
TiO_2	90.15	0.148	6.46
Ni/TiO_2	87.11	0.146	5.72

## 3. Results and discussion

3.1. Catalyst characterization

The phase structures of the prepared Ni/TiO_2 catalyst were investigated by powder X-ray diffraction (XRD). As shown in Fig. 1a, in the XRD patterns of the Ni/TiO_2 catalyst, the TiO_2 presents the structure of a major anatase phase, together with a minor rutile and brookite, which is consistent with the TiO_2 support. The characteristic peaks assigning to the Ni species are not detected in the XRD patterns of Ni/TiO_2 sample, indicating the homogeneous dispersion of Ni metal on TiO_2 support. The UV–vis diffuse reflectance spectrum (DRS) was measured to determine the optical properties of the Ni/TiO_2 catalyst. As seen in Fig. 1b, no obvious changes in the light response of Ni/TiO_2 were observed as compared with the bare TiO_2 support. Furthermore, the results of N_2 physisorption measurements (seen in Table 1) demonstrate that the BET surface area, pore volume, and pore diameter of the Ni/TiO_2 catalyst have minor declines compared with the TiO_2 support.

Transmission electron microscopy (TEM) characterizations were conducted to examine the morphologies of the Ni/TiO_2 catalyst. As displayed in Fig. 2a, well dispersed NiO nanoparticles with sizes of 8–15 nm are deposited on the surface of TiO_2 support. In the high-resolution TEM image (Fig. 2b), the lattice fringes with d-spacing of 0.208 nm and 0.351 nm are indexed to the {2 0 0} lattice plane of NiO and the {1 0 1} lattice plane of anatase, respectively. These findings reflect that the Ni spices on the surface of TiO_2 are oxidized to NiO due to the inevitable contact of the catalyst with air before TEM measurements.

To provide detailed information about the electronic properties of the surface elements, the prepared Ni/TiO_2 catalyst was studied by XPS characterization and the results are presented in Fig. S2. The survey spectrum (Fig. S2a) gives the signals of Ni, Ti, and O elements only, suggesting the purity of the Ni/TiO_2 sample. The two peaks observed in the high-resolution spectrum of Ti 2p are correspondingly assigned to Ti $2p_{1/2}$ and Ti $2p_{3/2}$. In the Ni $2p_{3/2}$ high-resolution spectrum (Fig. S2c), the peak with binding
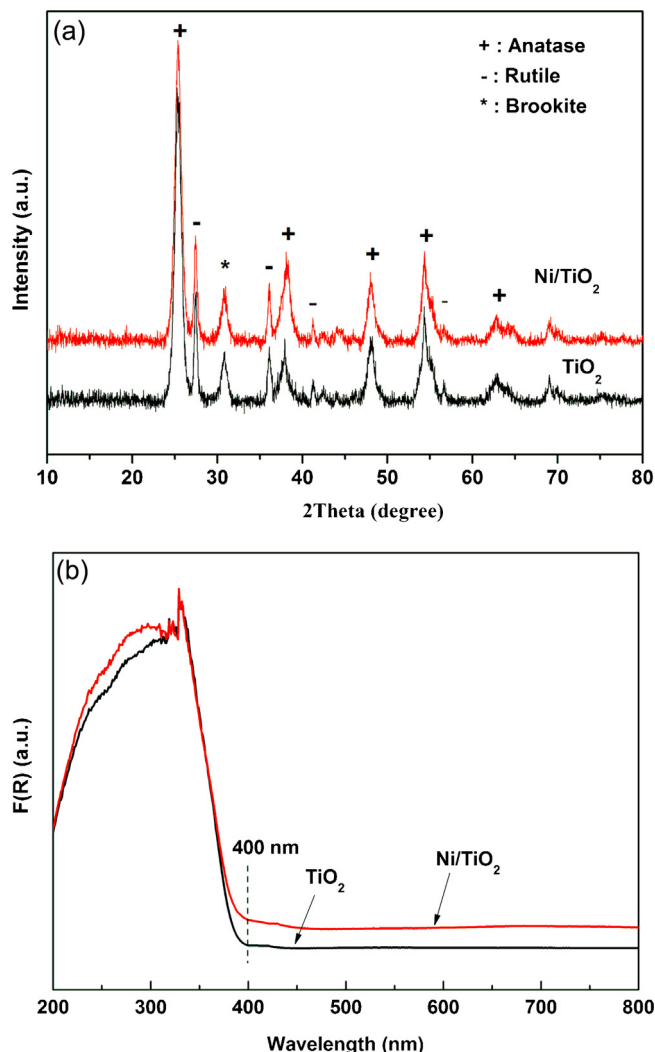
Fig. 1. (a) XRD patterns and (b) DRS spectra of Ni/TiO_2 and TiO_2 samples.

energy of 854.4 eV together with the broad shake-up satellite peak at around 860.0 eV is characteristic of NiO species [45], indicating the surface Ni species were oxidized to NiO during the sample transfer before the XPS measurement, consistent with the result of
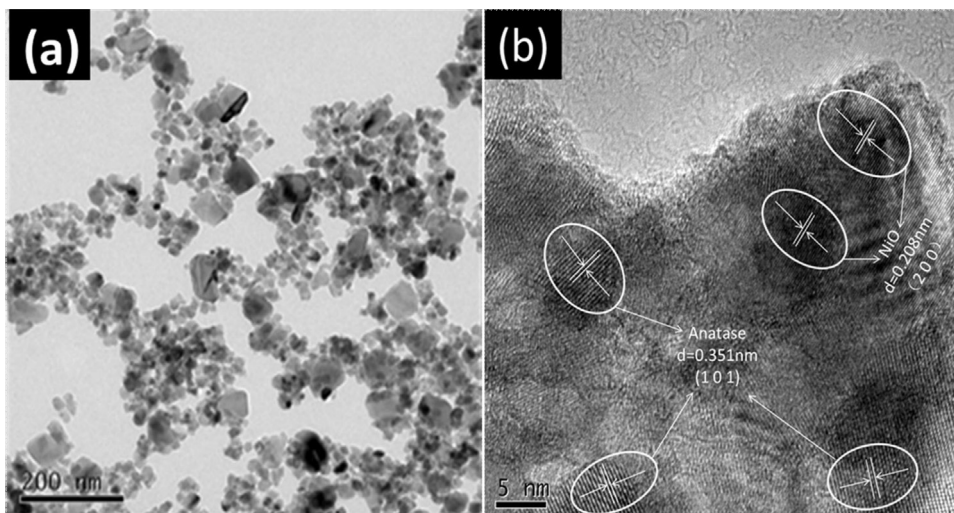
Fig. 2. Typical TEM image (a) and the high-resolution TEM image (b) of Ni/TiO_2 sample.
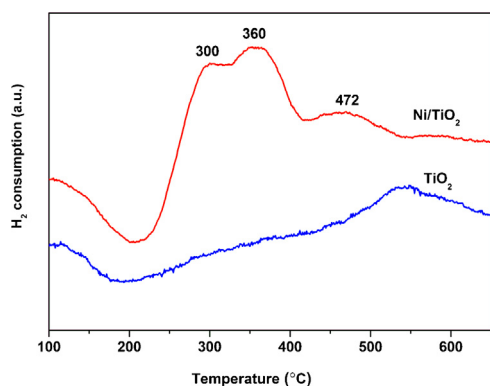
Fig. 3. H$_2$-TPR profiles of TiO$_2$ and Ni/TiO$_2$ samples.

TEM. The broad O 1s spectrum in Fig. S2d can be fitted into three sub-peaks with binding energy of 529.6, 530.7 and 531.8 eV, which are attributed to the lattice oxygen in TiO$_2$, the lattice oxygen in NiO, and the surface hydroxyl oxygen in TiO$_2$, respectively [46].

As the results of TEM and XPS measurements, the Ni spices on the surface of the Ni/TiO$_2$ catalyst are indeed readily oxidized to NiO as exposure to air, H$_2$ temperature-programmed reduction (TPR) tests were thus carried out to explore the proper reduction temperature for reducing the Ni/TiO$_2$ catalyst to ensure that the possible oxidized Ni is fully reduced before photo-thermal or thermal catalytic reactions. Fig. 3 shows the H$_2$-TPR profiles of TiO$_2$ support and Ni/TiO$_2$ catalyst. The pure TiO$_2$ support exhibits a reduction temperature at about 540 °C. In the case of Ni/TiO$_2$, three reduction peaks at about 300, 360 and 472 °C are observed. The two former reduction peaks at the relative low temperatures are attributed to the reduction of NiO that holds significant interactions with TiO$_2$ support to metallic Ni. The high reduction peak at about 472 °C is due to the partial reduction of TiO$_2$ support [18,38,47]. From the results of TPR tests, it is confirmed that, after reduced by the H$_2$/He stream at 300 °C, the Ni species in Ni/TiO$_2$ are in the Ni^0 state, precluding the possible influence of NiO in the selective CO methanation reaction.

3.2. Catalytic performance

The catalytic performance of CO methanation over the Ni/TiO$_2$ catalyst was first investigated in various H$_2$-rich streams. As shown in Fig. 4, introducing UV light into the catalytic systems can markedly enhance the conversion of CO in H$_2$-rich atmospheres. Moreover, this promotional effect of UV light for the hydrogenation of CO to CH$_4$ increases with the increase in H$_2$ concentration,
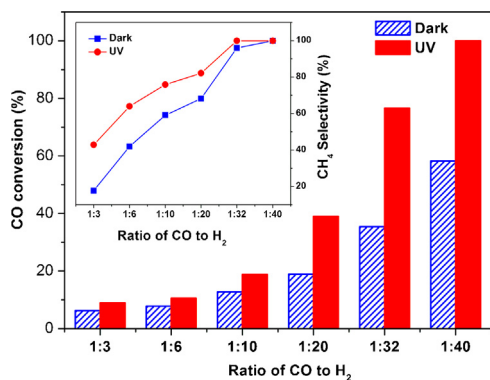

Fig. 4. Studies on the catalytic performance of CO methanation in various H$_2$-rich streams over 1.0 wt% Ni/TiO$_2$ catalyst at 250 °C under UV light irradiation and in dark.
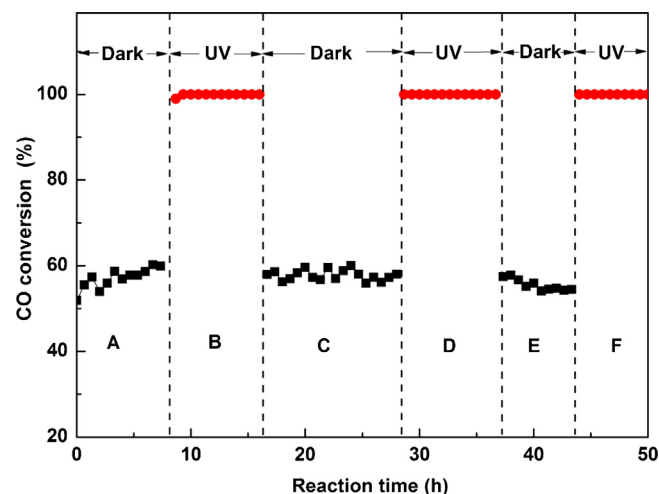

Fig. 5. CO conversion as a function of reaction time over Ni/TiO$_2$ catalyst at 250 °C under UV irradiation and in dark.

and a completed CO conversion is achieved in the reaction stream with a CO/H$_2$ ratio of 1/40 under UV irradiation. Noteworthy, with the introduction of UV light irradiation, the selectivity of CH$_4$ formation is also evidently enhanced. At the CO/H$_2$ ratio of 1/40, all CO are converted into CH$_4$ (100% CH$_4$ selectivity) under UV irradiation. These results indicate that UV light can remarkably promote the CO methanation over Ni/TiO$_2$ catalyst.

To investigate the stability of the promotional effect of UV light on CO hydrogenation over Ni/TiO$_2$, the reaction was alternately operated under UV irradiation and in dark in the stream with CO/H$_2$ ratio of 1/40 at 250 °C. As seen in Fig. 5, once UV light is introduced into the reaction system (process B), the CO conversion is increased from about 60% in dark (process A) up to 100%. With the removal of UV light (process C), the conversion of CO is reduced down to 60% again. This phenomenon occurs as well in the following cycles with UV light (process D and F) irradiation and in dark (process E). Notes that the CO conversion seems to decrease slightly in dark during the process E, but always keeps at 100% under UV irradiation during the process D and F. This observation indicates that UV light can also promote the stability of CO methanation over Ni/TiO$_2$. Note that the thermo-catalytic stability over Ni/TiO$_2$ is far lower than that of Ru/TiO$_2$ in our previous work [43], but UV irradiation can keep the high activity of Ni/TiO$_2$, similarly to that of Ru/TiO$_2$. This shows that the enhanced effect of UV irradiation over Ni/TiO$_2$ is superior to that over Ru/TiO$_2$.

However, no enhancement in CO conversion or CH$_4$ selectivity was observed under visible light ($\lambda > 420$ nm) irradiation (results not presented). Because the UV light of 300 ~ 420 nm used in this work can only induce the optical response of TiO$_2$, but not Ni or NiO nanoparticles, the promoted effect of UV light on CO methanation over Ni/TiO$_2$ can be only attributed to the band-gap excitation of TiO$_2$ support.

In the reported works [43,48], we have presented that the photo-generated electrons induced by the band-gap excitation of TiO$_2$ under UV irradiation can transfer from the conduction band of TiO$_2$ to adjacent Au or Ru sites, rendering the Au or Ru nanoparticles with higher surface electron density and consequently facilitating the adsorption and activation of CO molecules. To interpret the promotional effect of UV light on the hydrogenation of CO to CH$_4$ over Ni/TiO$_2$, the surface states of Ni species and the chemisorption of CO at Ni sites over Ni/TiO$_2$ with UV irradiation or not were investigated by XPS and FT-IR measurements, respectively.

Fig. 6a shows the Ni 2p$_{2/3}$ high-resolution XPS spectra of the reacted Ni/TiO$_2$ sample under UV irradiation or in dark. As can be seen, the Ni species exist in the state of Ni^{2+} in the two samples,
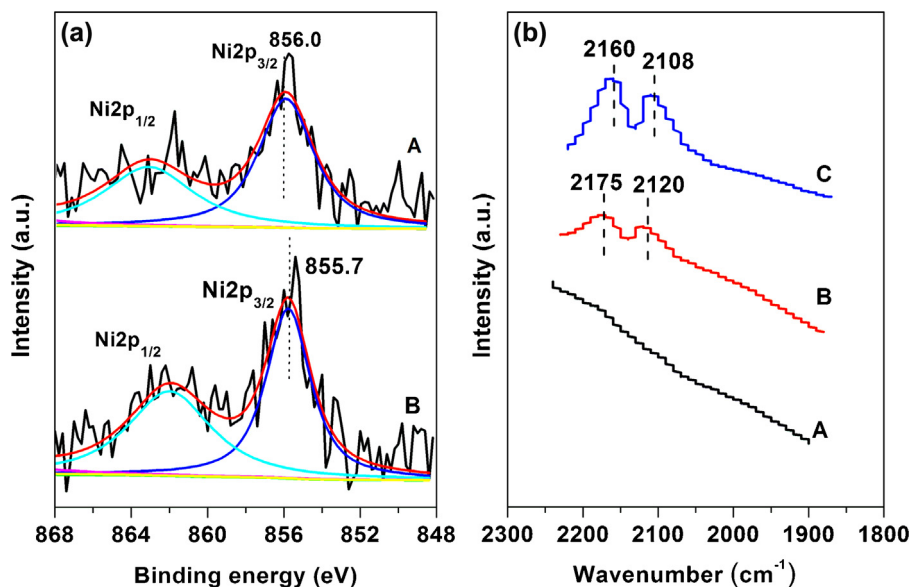
Fig. 6. (a) Ni $2p_{2/3}$ high-resolution XPS spectrum of Ni/TiO$_2$ sample after reacting at 250 °C for 24 h (A) indark or (B) under UV irradiation. (b) FT-IR spectra of CO adsorption over Ni/TiO$_2$ sample: (A) before gas adsorption, (B) after CO adsorption in dark, and (C) after CO adsorption under UV irradiation.(For interpretation of the references to color in text, the reader is referred to the web version of this article.)

and almost no Ni^0 was observed, which can be attributed to the oxidation of metallic Ni speices due to the exposure to air before XPS testing. Comparing with the Ni $2p_{3/2}$ spectra of the as-prepared Ni/TiO$_2$ catalyst before reaction (Fig. S2c), an increase in the binding energy (BE) of Ni $2p_{3/2}$ was observed for the reacted Ni/TiO$_2$ sample (BE shifted from 855.4 to 856 eV) in dark (the top curve A in Fig. 6a). This can be attributed to the enhanced interaction between the Ni species and TiO$_2$ support during the thermocatalytic reaction process [49]. However, the binding energy of Ni $2p_{3/2}$ of the reacted Ni/TiO$_2$ sample (BE = 855.7 eV, the bottom curve B in Fig. 6a,) under UV irradiation is less than that of the reacted sample in dark, indicating a higher surface electron density of Ni species under UV irradiation. Here, the photo-generated electrons induced by the band-gap excitation of TiO$_2$ under UV irradiation can transfer to the adjacent Ni sites.

Moreover, we have ever found that the increase in the surface electron density of TiO$_2$-supported metals (e.g., Au, Pt, and Ru) could promote the chemisorption of CO and its activation at metal sites in our previous work [42,43,50]. Following this viewpoint, we think that the increased surface electron density of Ni metal over Ni/TiO$_2$ induced by UV light maybe also promote the chemisorption and activation of CO at Ni sites. To confirm it, we have further investigated the CO adsorption behavior of Ni/TiO$_2$ under UV irradiation or not by FT-IR characterizations. As seen in Fig. 6b, after the Ni/TiO$_2$ sample absorbing CO without UV irradiation, two peaks at about 2120 and 2175 cm^{-1} were detected (the red curve B in Fig. 6b), corresponding to the carbonyl stretching vibration of linear CO molecules coordinated to Ni nanoparticles. With the introduction of UV irradiation, two increased CO adsorption peaks at Ni sites are observed at about 2108 and 2160 cm^{-1} (the blue curve C in Fig. 6b), respectively, which are in lower frequency compared with that of in dark condition. This indicates that UV light can firmly enhance the adsorption and activation of CO at Ni sites over Ni/TiO$_2$ catalyst.

The above FT-IR results over Ni/TiO$_2$ can be explained as follows: with UV light excitation, the photo-generated electrons in the conduction band of TiO$_2$ can transfer into the d orbital of Ni, causing the Ni sites with increased surface electron density (seen in Fig. 6a). Then, the rich d-electrons in Ni can transfer to the π^* orbital of CO molecule adsorbed at Ni sites (Ni–C≡O) according to

the d–π^* back-donation principle [42,51]. Consequently, the bond of Ni–C is strengthened, while the C–O bond is weakened. Therefore, more CO molecules are adsorbed and activated at Ni sites of Ni/TiO$_2$ under UV irradiation.

To further elucidate the promotion effect of the enhanced adsorption and activation of CO at Ni sites on the methanation of CO over Ni/TiO$_2$, the process of the thermal-catalytic CO methanation needs to be known. Although some different reaction mechanisms are proposed for the CO methanation over nickel supported catalyst [30–38], it is a broad consensus that the surface-adsorbed carbon species (Ni–C), formed by the dissociated adsorption of CO, is a key intermediate species during the process of CO methanation. This
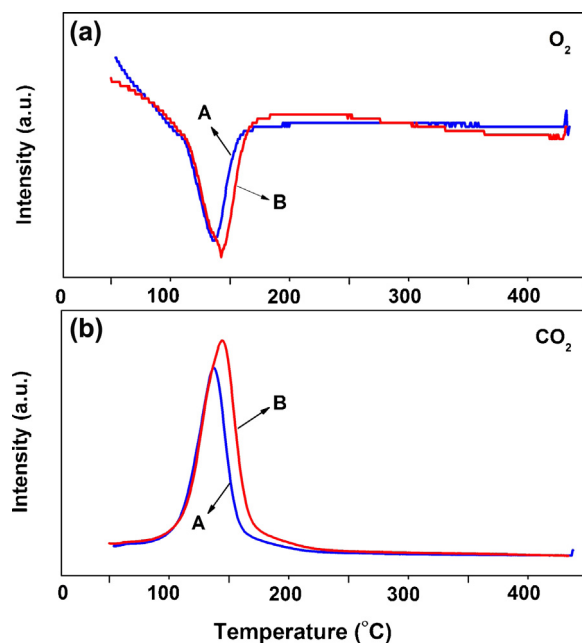

Fig. 7. (a) O$_2$ consumption and (b) CO$_2$ formation mass signal during the TPO process over the reacted Ni/TiO$_2$ sample (A) in dark or (B) under UV irradiation. (For interpretation of the references to color in text, the reader is referred to the web version of this article.)

Ni—C species will further react with the adsorbed hydrogen to form CH_4. Obviously, the activation of CO adsorbed at Ni sites induced by UV light will benefit to the formation of Ni—C species (the broken of C—O bond), which further promote the CO methanation according to the mentioned mechanism. In fact, this explanation seems to be confirmed by the following TPO testing over the reacted Ni/TiO_2 sample under UV irradiation or not.

Fig. 7 shows the mass signal curves of O_2 consumption and CO_2 formation during the process of TPO testing. An obvious increase in mass signal of O_2 consumption was observed over the reacted Ni/TiO_2 sample under UV irradiation (the red curve B in Fig. 7a) as compared with that of sample in dark (the blue curve A in Fig. 7a). Moreover, the intensity of mass signal of CO_2 formation over the reacted Ni/TiO_2 sample under UV irradiation (the red curve B in Fig. 7b) is also evidently stronger than that of sample in dark (the blue curve A in Fig. 7b). The results indicate that the amount of surface carbon species adsorbed at Ni sites (Ni—C, an intermediate species) over Ni/TiO_2 are clearly increased with the introduction of UV light into the reaction system; which thus, supports the above conclusion that the photo-assisted effect on CO dissociation at Ni sites is involved within the CO methanation over Ni/TiO_2 under UV irradiation. Based on the above mentioned results and analysis, the probable extra process of CO hydrogenation to CH_4 over Ni/TiO_2 under UV irradiation can be described as follows.

(1) The photo-induced charge carriers (e_{cb}^- and h_{vb}^+) are formed at the surface of TiO_2 support under UV irradiation:

$$TiO_2 + h\nu \rightarrow TiO_2(e_{cb}^-, h_{vb}^+)$$

(2) The photo-generated electrons transfer from TiO_2 to the adjacent Ni sites, leading to the increase in surface electron density of Ni, and consequently the promoted adsorption and activation of CO molecules at Ni sites:

$$Ni + TiO_2(e_{cb}^-) \rightarrow TiO_2 + Ni(e^-)$$

$$Ni(e^-) + CO \rightarrow \{Ni—C≡O\}$$
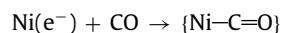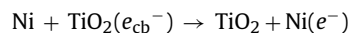
(3) The activated CO strongly interacts with the dissociated H to from the surface carbon species adsorbed at Ni sites (Ni—C):

$$\{Ni—C≡O\} + Ni—H \rightarrow Ni—C + H_2O$$
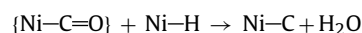
(4) Ni—C species reacts with Ni—H to form CH_4:

$$Ni—C + 4Ni—H \rightarrow Ni + CH_4$$
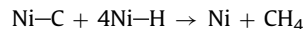
During the above process, it is mainly the promoted adsorption and activation of CO molecules at Ni sites induced by electron transfer from TiO_2 to Ni under UV irradiation to be responsible for the enhanced methanation. The above proposed mechanism of CO methanation over Ni/TiO_2 under UV irradiation can also be described in Fig. 8. This study implies that the photo-generated electrons induced by the band-gap excitation of TiO_2 can be acted as electron donor (instead of the traditional electron additives) to promote the thermal catalytic hydrogenation of CO to CH_4 over the TiO_2 supported noble-metal-free catalyst Ni/TiO_2.

Although our previous work [43] has presented the promoted effect of UV light on the thermo-catalytic methanation of CO over Ru/TiO_2, this work still shows its value and difference: (I) Ni/TiO_2 is a non-noble-metal, cheaper, more eco-friendly catalyst than Ru/TiO_2; and thus, holds a greater potential for the practical application than the latter. (II) This work has confirmed the knowledge and the methodology delivered by the work of Ru/TiO_2, which may be further extend to other TiO_2 supported metal catalysts, provided that the work function value of metal is higher than that of TiO_2. (III) The enhanced effect of UV irradiation on the activity and stability of CO methanation over Ni/TiO_2 is superior to that over Ru/TiO_2, exhibiting a potential application for Ni/TiO_2. In addition, the TPO
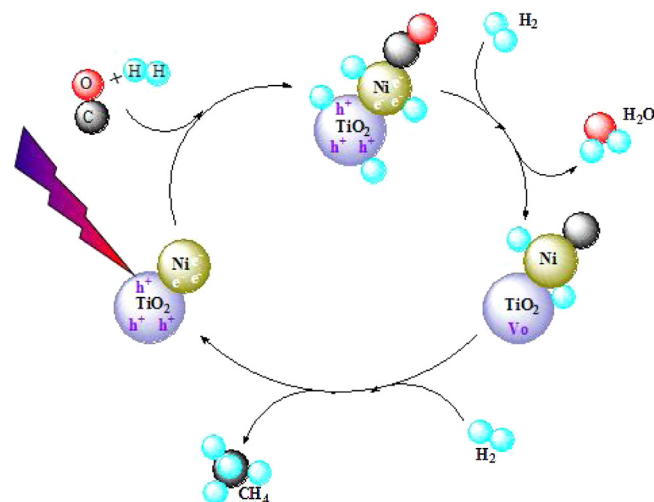

Fig. 8. Schematic of reaction process of CO methanation over Ni/TiO_2 under UV irradiation.

testing can also demonstrate the formation of the surface intermediate species over catalyst instead of the temperature programmed surface reaction (TPSR) testing.

4. Conclusions

Introduction of UV light can remarkably promote the thermal catalytic activity and its stability of Ni/TiO_2 for CO methanation in the rich-H_2 stream. Based on the results of XPS, FT-IR, and TPO characterizations, it is proposed that this promotion of UV light in hydrogenation of CO to CH_4 can be mainly stemmed from the photo-generated electron transfer from TiO_2 support to the adjacent Ni sites, resulting in the increase in surface electron density of Ni metals and the subsequent enhanced adsorption and activation of CO molecules at Ni particles. Furthermore, the activated CO molecules will be formed into the surface carbon species adsorbed at Ni sites (Ni—C, as the active species), and then promote the methanation of CO. This study shows that the promoted effect of UV light on the thermal catalytic methanation of CO not only occurs on the TiO_2 supported noble metal catalyst (e.g., Ru/TiO_2), but also the TiO_2 supported noble-metal-free catalyst (e.g., Ni/TiO_2).

Appendix A. Supplementary data

Supplementary data associated with this article can be found, in the online version, at http://dx.doi.org/10.1016/j.apcatb. 2014.12.049.

References

[1] L. Carrette, K.A. Friedrich, U. Stimming, Fuel Cells 1 (2001) 5–39.
[2] A.K. Shukla, A.S. Aricò, V. Antonucci, Renew. Sustain. Energy Rev. 5 (2001) 137–155.
[3] R. Moy, Science 301 (2003) 47.
[4] Y. Men, G. Kolb, R. Zapf, V. Hessel, H. Löwe, Catal. Today 125 (2007) 81–87.
[5] S. Takenaka, K. Kawashima, H. Matsune, M. Kishida, Appl. Catal. A: Gen. 321 (2007) 165–174.
[6] A.F. Ghenciu, Curr. Opin. Solid State Mater. Sci. 6 (2002) 389–399.

[7] S. Gamburzev, A.J. Appleby, J. Power Sources 107 (2002) 5–12.
[8] M.B.I. Choudhury, S. Ahmed, Appl. Catal. A: Gen. 314 (2006) 47–53.
[9] Q. Liu, L. Liao, Z. Liu, Chin. J. Chem. Eng. 19 (2011) 434–438.
[10] L. Shore, R.J. Farrauto, W. Vielstich, A. Lamm, H.A. Gasteiger (Eds.), Handbook of Fuel Cells: Fundamentals Technology and Applications, 3, John Wiley & Sons Ltd., West Sussex, 2003, p. 211.
[11] S.H. Oh, R.M. Sinkevitch, J. Catal. 142 (1993) 254–262.
[12] C.D. Dudfield, R. Chen, P.L. Adcock, Int. J. Hydrogen Energy 26 (2001) 763–775.
[13] O. Korotkikh, R. Farrauto, Catal. Today 62 (2000) 249–254.
[14] G. Xu, X. Chen, Z.G. Zhang, Chem. Eng. J. 121 (2006) 97–107.
[15] R.W. McCabe, P.J. Mitchell, J. Catal. 103 (1987) 419–425.
[16] V. Jayaraman, Y.S. Lin, J. Membr. Sci. 104 (1995) 251–262.
[17] E.D. Park, D. Lee, H.C. Lee, Catal. Today 139 (2009) 280–290.
[18] M. Krämer, M. Duisberg, K. Stöwe, W.F. Maier, J. Catal. 251 (2007) 410–422.
[19] S. Takenaka, T. Shimizu, K. Otsuka, Int. J. Hydrogen Energy 29 (2004) 1065–1073.
[20] O. Görke, P. Pfeifer, K. Schubert, Catal. Today 110 (2005) 132–139.
[21] M.B.I. Choudhury, S. Ahmed, M.A. Shalabi, T. Inui, Appl. Catal. A: Gen. 314 (2006) 47–53.
[22] P. Panagiotopoulou, D.I. Kondarides, X.E. Verykios, Appl. Catal. A: Gen. 344 (2008) 45–54.
[23] T. Utaka, T. Takeguchi, R. Kikuchi, K. Eguchi, Appl. Catal. A: Gen. 246 (2003) 117–124.
[24] S. Eckle, Y. Denkwitz, R.J. Behm, J. Catal. 269 (2010) 255–268.
[25] R.A. Dagle, Y. Wang, G.G. Xia, J.J. Strohm, J. Holladay, D.R. Palo, Appl. Catal. A: Gen. 326 (2007) 213–218.
[26] S. Tada, R. Kikuchi, A. Takagaki, T. Sugawara, S.T. Oyama, S. Satokawa, Catal. Today 232 (2014) 16–21.
[27] P. Panagiotopoulou, D.I. Kondarides, X.E. Verykios, Appl. Catal. B: Environ. 88 (2009) 470–478.
[28] A. Chen, T. Miyao, K. Higashiyama, H. Yamashita, M. Watanabe, Angew. Chem. Int. Ed. 49 (2010) 9895–9898.
[29] P. Panagiotopoulou, D.I. Kondarides, X.E. Verykios, J. Phys. Chem. C 115 (2010) 1220–1230.
[30] D. Hu, J. Gao, Y. Ping, L. Jia, P. Gunawan, Z. Zhong, G. Xu, F. Gu, F. Su, Ind. Eng. Chem. Res. 51 (2012) 4875–4886.
[31] C. Mirodatos, H. Praliaud, M. Primet, J. Catal. 107 (1987) 275–287.
[32] M.M. Zyryanova, P.V. Snytnikov, R.V. Gulyaev, Y.I. Amosov, A.I. Boronin, V.A. Sobyanin, Chem. Eng. J. 238 (2014) 189–197.
[33] Q. Liu, X. Dong, X. Mo, W. Lin, J. Nat. Gas Chem. 17 (2008) 268–272.
[34] H. Yoshida, K. Watanabe, N. Iwasa, S. Fujita, M. Arai, Appl. Catal. B: Environ. 162 (2015) 93–97.
[35] V.M. Shinde, G. Madras, AIChE J. 60 (2014) 1027–1035.
[36] S. Tada, R. Kikuchi, A. Takagaki, T. Sugawara, S.T. Oyama, K. Urasaki, S. Satokawa, Appl. Catal. B: Environ. 140–141 (2013) 258–264.
[37] K. Urasaki, Y. Tanpo, Y. Nagashima, R. Kikuchi, S. Satokawa, Appl. Catal. A: Gen. 452 (2013) 174–178.
[38] S. Tada, R. Kikuchi, K. Wada, K. Osada, K. Akiyama, S. Satokawa, Y. Kawashima, J. Power Sources 264 (2014) 59–66.
[39] Z.G. Zhang, G. Xu, Catal. Commun. 8 (2007) 953–956.
[40] L. Fan, N. Ichikuni, S. Shimazu, U. Takayoshi, Appl. Catal. A: Gen. 246 (2003) 87–95.
[41] H. Hakkinen, U. Landman, J. Am. Chem. Soc. 123 (2001) 9704–9705.
[42] H.R. Zheng, H.Y. Yang, R.R. Si, W.X. Dai, X. Chen, X.X. Wang, P. Liu, X.Z. Fu, Appl. Catal. B: Environ. 105 (2011) 243–247.
[43] X.H. Lin, K. Yang, R.R. Si, X. Chen, W.X. Dai, X.Z. Fu, Appl. Catal. B: Environ. 147 (2014) 585–591.
[44] W.X. Dai, X.X. Wang, P. Liu, Y.M. Xu, G.S. Li, X.Z. Fu, J. Phys. Chem. B 110 (2006) 13470–13476.
[45] P. Girault, J. Grosseau-Poussard, J. Dinhut, L. Marechal, Nucl. Instrum. Methods Phys. Res. Sect. B 174 (2001) 439–452.
[46] E.L. Bullock, L. Patthey, S.G. Steinemann, Surf. Sci. 352–354 (1996) 504–510.
[47] P.M. Sreekanth, P.G. Smirniotis, Catal. Lett. 122 (2008) 37–42.
[48] K. Yang, J. Liu, R. Si, X. Chen, W. Dai, X. Fu, J. Catal. 317 (2014) 229–239.
[49] C. Jia, J. Gao, J. Li, F. Gu, G. Xu, Z. Zhong, F. Su, Catal. Sci. Technol. 3 (2013) 490–499.
[50] W.X. Dai, X.P. Zheng, H.Y. Yang, X. Chen, X.X. Wang, P. Liu, X.Z. Fu, J. Power Sources 188 (2009) 507–514.
[51] G. Blyholder, J. Phys. Chem. 68 (1964) 2772–2777.